Response to referee comments on "An Integrated Synchronous Online Analyzer for Gaseous and Particulate Reactive Oxygen Species (ROS): Development, Characterization and Field Observations"

We sincerely thank the editors and the reviewers for their valuable comments and constructive suggestions on our manuscript. These comments have been very helpful in improving the quality, clarity, and scientific rigor of the manuscript. We have carefully considered all comments and revised the manuscript accordingly. The main revisions and our point-by-point responses to the reviewer's comments are provided below. The reviewer's comments are shown in black, our responses in **blue**, and the text added to the revised manuscript in ***blue italics***.

Response to Anonymous Referee #2:

This manuscript presents an integrated online analyzer for the synchronous measurement of gaseous and particulate reactive oxygen species, based on the DCFH-HRP fluorescence method, together with a four-season field campaign in Beijing. The synchronous dual-phase capability and the seasonal dataset are useful contributions. However, several issues regarding methodological rigor, the reliability of key performance metrics, and the interpretation of the field data should be addressed.

Major Comments:

Comment 1: Definition and chemical selectivity of the measurement. The DCFH-HRP system responds very differently to different ROS species, and after wet-chemical absorption the instrument effectively quantifies only the water-soluble, DCFH-reactive subset of ROS. I suggest the authors state explicitly what operationally-defined quantity is measured, and revise the wording in the Abstract and Conclusions (e.g., "DCFH-reactive water-soluble ROS, as H_2O_2 equivalents") so the values are not read as total ROS.

Response 1: We thank the reviewer for this important comment. We agree that ambient ROS consists of a complex mixture of peroxides, radicals, and other oxidants, and that the DCFH-HRP assay does not respond equally to different ROS species. Accordingly, the ROS concentrations calibrated with H_2O_2

standards should not be interpreted as molecule-specific concentrations or as the total abundance of all atmospheric ROS.

To address this issue, we revised the manuscript to clarify the operational meaning of the reported ROS concentrations and the chemical selectivity of the DCFH-HRP assay. In the **Abstract**, we specified that the measured ROS_g and ROS_p concentrations are reported as H_2O_2 equivalents. In Sect. **2.2 Instrument principle**, we added a discussion of the species-dependent response of the DCFH-HRP assay, noting that previous characterization showed a response of peracetic acid close to that of H_2O_2, but much lower relative sensitivities for sterically hindered organic peroxides, including tert-butyl hydroperoxide, benzoyl peroxide, lauroyl peroxide, and 2-butanone peroxide. This section also clarifies that ROS species with low reactivity toward the DCFH-HRP system or limited aqueous stability may contribute less efficiently to the fluorescence signal, leading to species-dependent response biases. In Sect. **2.4 Instrument calibration**, we added a statement that the calibrated ROS concentrations represent operational H_2O_2-equivalent responses rather than absolute or molecule-specific quantification of total atmospheric ROS. The opening sentence of Sect. **5 Conclusions** was also revised to maintain this terminology consistently throughout the manuscript.

Revision in the manuscript:

The following text was revised in Abstract (line 10-11):

An integrated online analyzer was developed for in situ, synchronous quantification of gaseous and particulate reactive oxygen species (ROS), with concentrations reported as H_2O_2 equivalents.

The following text was added to Sect. 2.2 Instrument principle (line 119-126):

It should be noted that the DCFH-HRP assay is not equally sensitive to all ROS species. Previous characterization of DCFH-based atmospheric ROS measurements showed that peracetic acid produced a response close to that of H_2O_2, whereas sterically hindered organic peroxides, such as tert-butyl hydroperoxide, benzoyl peroxide, lauroyl peroxide, and 2-butanone peroxide, exhibited much lower relative sensitivities (Zhou et al., 2018). Therefore, the measured signal represents an operationally defined fraction of water-soluble, DCFH-reactive oxidants expressed as H_2O_2 equivalents, rather than the total abundance of all atmospheric ROS. Consequently, ROS species with low DCFH-HRP reactivity

or limited aqueous stability may contribute less efficiently to the fluorescence signal, resulting in species-dependent response biases.

The following text was added to Sect. 2.4 Instrument calibration (line 181-183):

All measured ROS concentrations are expressed as H_2O_2 equivalents and should therefore be regarded as operationally defined ROS responses rather than absolute or molecule-specific quantification of total atmospheric ROS.

The following text was revised in Sect. 5 Conclusions (line 572-573):

This study developed an integrated online analyzer for synchronous quantification of ROS_g and ROS_p, reported as H_2O_2-equivalent concentrations.

Comment 2: Collection efficiencies (γ_p). Eq. 2.5 includes M_{wall} (wall-deposited material) in the numerator, but this fraction is recovered only by offline rinsing and does not enter the detection path during routine operation. The effective online efficiency would be closer to 81.72%, implying the reported ROS_p values may be underestimated by ~10%. Please either (1) adopt M_{col} / (M_{col} + M_{wall} + M_{filter}) as the collection efficiency and revise the ROS_p values throughout the manuscript accordingly, (2) demonstrate that wall deposits could be eventually detected, or (3) explicitly discuss the direction and magnitude of this bias.

Response 2: We are very thankful for the reviewer's careful and important comment. We agree that the wall-deposited fraction should not be included in the effective online collection efficiency because this fraction was recovered only by offline rinsing and did not enter the online fluorescence detection path during routine operation. In the original manuscript, the value of 91.2% was intended to describe the overall chamber retention including the wall-deposited fraction, but we agree that it is not appropriate for correcting online ROS_p concentrations.

To address this issue, we revised the definition and application of γ_p in Sect. **2.4 Instrument calibration**, and clarified the particle collection process in Sect. **2.3.1 Sample collection process**. The effective online collection efficiency is now defined as: $\gamma_p = \frac{M_{col}}{M_{col}+M_{wall}+M_{filter}}$ (Eq. 2.5), where M_{col} is the chamber-collected liquid directly delivered to the detector, M_{wall} is the wall-rinse fraction, and M_{filter} is the

downstream backup filter fraction. Based on the recovery experiment, 81.72% of the recovered amount was present in the chamber-collected liquid, 9.46% was recovered from wall rinsing, and 8.80% was found on the downstream backup filter. Therefore, γ_p = 81.72% was adopted for ROS_p quantification in the revised manuscript, while the wall-rinse fraction was treated as a sampling loss rather than an online-detected fraction.

Accordingly, we recalculated all ROS_p-related values throughout the manuscript and Supplement. These revisions were made in the **Abstract**, Sect. **3.2.1 Baseline stability and detection Limit**, Sect**. 3.2.3 Sensitivity and response time**, Sect. **3.2.4 Linear working range**, Sect. **4.2 Overall variations of ROS and associated atmospheric species**, **Fig. 3**, **Tables 2 and 3**, **Figs. 4 and 5**, and Supplementary **Tables S2 and S3**. The recalculated ROS_p concentrations were approximately 11.6% higher than the originally reported values. Because this correction is a constant scaling factor, the seasonal ranking, diurnal patterns, pollution-regime dependence, correlations, and main conclusions remain unchanged.

Revision in the manuscript:

The following text was revised in Abstract (line 15-17):

The system achieved high stability (RSD 0.37% over 10 h), fast tracking (7 min response), good repeatability (RSD 0.57%, n=10), and robust linearity (y≈0.1x, R^2=0.99) with detection limits of 0.07 ppbv (ROS_g) and 0.007 μg m^{-3} (ROS_p) expressed as H_2O_2 equivalents

The following text was revised in Sect. 2.3.1 Sample collection process (line 155-156):

The high-speed airflow carries the particles to the chamber exit, achieving an 81.72% collection efficiency.

The following text was revised in Sect. 2.4 Instrument calibration (line 211-219):

$$\gamma_p = \frac{M_{col}}{M_{col} + M_{wall} + M_{filter}} \quad (2.5)$$

The recovery experiment was conducted in triplicate under actual ambient aerosol sampling conditions. The mean recovered fractions were 81.72% in the chamber-collected liquid, 9.46% in the wall-rinse solution, and 8.80% on the downstream backup filter. The wall-rinse and backup-filter fractions were

used to evaluate wall deposition and particle breakthrough, respectively. Since only the chamber-collected liquid was directly delivered to the second premixing chamber during routine online operation, γ_p = 81.72% was used as the effective online collection efficiency for ROS_p quantification in Eq. (2.4). This value represents an operational mean collection efficiency for the present field deployment. Potential variations associated with particle loading, hygroscopic growth, aerosol chemical composition, and long-term operation should be further evaluated in future applications.

The following text was revised in Sect. 3.2.1 Baseline stability and detection Limit (line 285-286):

The detection limit was derived using the 3σ criterion based on baseline noise, yielding 0.07 ppbv for ROS_g and 0.007 μg m^{-3} for ROS_p.

The following text was revised in Sect. 3.2.3 Sensitivity and response time (line 295-296):

Standards of 5.0, 10.0, 20.0, and 25.0 μg L^{-1} correspond to ROS_g of 2.88, 5.76, 11.52, and 14.41 ppbv, and ROS_p of 0.33, 0.66, 1.33, and 1.66 μg m^{-3}.

The following text was revised in Sect. 3.2.4 Linear working range (line 305-306):

The atmospheric-equivalent calibration range was 2.88-14.41 ppbv for ROS_g and 0.33-1.66 μg m^{-3} for ROS_p.

The following text was revised in Sect. 4.2 Overall variations of ROS and associated atmospheric species (line 399-401):

Notably, ROS_g and ROS_p exhibited a consistent seasonal pattern, with maximum values in spring (2.28 ppbv and 0.50 μg m^{-3}, respectively) and minimum values in autumn (1.03 ppbv and 0.17 μg m^{-3}, respectively).

All ROS_p-related values in Fig. 3, Tables 2 and 3, Figs. 4 and 5, and Supplementary Tables S2 and S3 were recalculated using γ_p = 81.72% and updated accordingly.

Comment 3: Interference assessment relies largely on the literature. Section 3.3 discusses O_3, NO, SO_2, and Fe interferences almost entirely from prior studies, without tests on this instrument. Since

the present configuration (pH 7.0, 10 μM DCFH, 2 units mL^{-1} HRP) differs from those works, I recommend adding at least some direct interference tests. Also, in lines 315–318, you mention that "In fluorescence-based H_2O_2 detection, SO_2 can interfere with fluorophore formation through acid-catalyzed reactions. This interference can be fully suppressed by adding formaldehyde." Please clarify whether formaldehyde is actually used for SO_2 suppression in this study; if so, it does not appear in the flow schematic.

Response 3: We appreciate the reviewer's constructive comment. We agree that the previous interference assessment relied largely on literature evidence and did not sufficiently reflect the present instrument configuration. To address this issue, we added direct interference experiments under the same DCFH-HRP conditions used in this study, namely pH 7.0, 10 μmol L^{-1} DCFH, 2 units mL^{-1} HRP, and 40 °C.

Specifically, a 3 μg L^{-1} H_2O_2 standard was used as the reference solution, and SO_2, NO, Fe^{2+}, and mixed interferents were introduced into the H_2O_2 matrix. The H_2O_2-only solution was used as the control, and the relative bias was calculated from the change in the measured H_2O_2 concentration. The tested conditions included SO_2 treatments, NO treatments, Fe^{2+} treatments, and two mixed-interferent conditions representing environmentally representative and high-level sensitivity scenarios.

The results are now presented in the newly added **Figure 4** and discussed in Sect. **3.3 Interference assessment**. NO produced negligible interference across the tested range, with biases from −1.02% to 0.04%. SO_2 showed a concentration-dependent negative effect, with minor biases at low levels but stronger negative biases of −10.00% and −29.97% at higher levels. Fe^{2+} caused a systematic negative bias from −0.05% to −7.53%, consistent with Fe(II)-driven Fenton-type H_2O_2 consumption. The mixed-interferent tests showed total biases of −3.23% under the environmentally representative condition and −11.03% under the high-level sensitivity condition.

We also quantified the potential influence of these interferences on the field observations. The environmentally representative mixed bias corresponds to approximately −0.056 ppbv for ROS_g and −0.006 μg m^{-3} for ROS_p, below the detection limits of the instrument. Therefore, the quantified interference was insufficient to alter the seasonal or pollution-regime interpretation of the present observations. The high-level mixed condition represents a conservative sensitivity scenario and indicates that high-SO_2 or Fe-rich environments may lead to underestimation of ROS.

O_3-related effects were also clarified in the revised manuscript. Previous DCFH-HRP studies reported negligible responses at 60–80 ppbv O_3 and a maximum H_2O_2 quantification error below 0.03 ppbv even at 100 ppbv O_3, whereas positive artifacts became important only under much higher O_3 levels. Since the observed O_3 levels during the present campaign were within the ambient-relevant range evaluated previously, O_3-related interference was considered a minor positive uncertainty. The added laboratory tests therefore focused on SO_2, NO, Fe^{2+}, and their mixtures, which represent the major potential negative interferences under the present configuration.

We have also clarified the formaldehyde issue. Formaldehyde was not used in the present flow configuration and therefore does not appear in the flow schematic. The previous statement implying that SO_2 interference was fully suppressed by formaldehyde has been removed. In the revised manuscript, SO_2-related effects are retained as a potential negative interference rather than assumed to be chemically suppressed.

Revision in the manuscript:

The following text and figure were revised in Sect. 3.3 Interference assessment (line 336-375):

Potential interferences in the DCFH-HRP assay may arise from direct probe oxidation, aqueous consumption of H_2O_2, or side reactions affecting DCF formation. For oxidizing gases, previous studies have shown that O_3 interference is generally weak under ambient-relevant conditions. The dissolved O_3 level estimated at ~40 ppbv is insufficient to produce measurable DCFH-based artifacts, and laboratory tests at 60-80 ppbv O_3 showed negligible responses (Huang et al., 2016; King and Weber, 2013). Field evaluations further indicated that even 100 ppbv O_3 produced a maximum H_2O_2 quantification error below 0.03 ppbv, whereas positive artifacts became important only under extremely elevated O_3 levels up to several hundred ppbv due to secondary oxidant formation (Lazrus et al., 1986; Montesinos et al., 2015). Since the O_3 levels observed in the present campaign were within the ambient-relevant range evaluated in these studies, O_3-related interference was considered a minor positive artifact in the gas-phase channel.

Reducing gases and soluble transition metals were more directly relevant to potential negative biases in the present DCFH-HRP configuration. NO has been reported to cause only weak H_2O_2 loss, whereas

SO_2 can suppress H_2O_2 detection through aqueous S(IV) chemistry with strong dependence on concentration and pH (Hua et al., 2008; Lazrus et al., 1986; Komazaki et al., 2001). Fe^{2+} can also consume H_2O_2 through Fenton-type reactions, while Fe^{3+} shows limited interference under comparable conditions (Kolthoff and Medalia, 1949; Zhou et al., 2018). Therefore, direct laboratory tests were conducted for SO_2, NO, Fe^{2+}, and their mixtures under the same reaction conditions as the analyzer. The interference tests used a 3 μg L^{-1} H_2O_2 standard as the reference solution, and the H_2O_2-only solution was used as the control. The tested atmospheric-equivalent levels included 0.5, 1, 10, and 25 ppbv for SO_2; 10, 25, 50, and 100 ppbv for NO; and 20, 80, 160, and 400 ng m^{-3} for Fe^{2+}. Two mixed conditions were further examined: Mix1, an environmentally representative mixed condition composed of 1 ppbv SO_2, 25 ppbv NO, and 80 ng m^{-3} Fe^{2+}, and Mix2, a high-level sensitivity condition composed of 10 ppbv SO_2, 100 ppbv NO, and 160 ng m^{-3} Fe^{2+}. As shown in Figure 4, NO produced negligible interference across the tested range, with biases from −1.02% to 0.04%. SO_2 showed a clear concentration-dependent negative effect. The biases were minor at 0.5 and 1 ppbv SO_2 (−0.20% and −0.23%) but increased to −10.00% and −29.97% at 10 and 25 ppbv SO_2, respectively, consistent with H_2O_2 consumption by dissolved S(IV). Formaldehyde was not used in the present flow configuration; therefore, SO_2-related effects were retained as a potential negative interference rather than assumed to be chemically suppressed.

Fe^{2+} also caused a systematic negative bias, increasing from −0.05% at 20 ng m^{-3} to −2.73%, −4.69%, and −7.53% at 80, 160, and 400 ng m^{-3}, respectively. This trend agrees with Fe(II)-driven Fenton-type H_2O_2 consumption. The mixed-interferent tests provided a direct estimate of total interference under coexisting soluble species. The total bias was −3.23% for Mix1 and −11.03% for Mix2, indicating that the combined effect was mainly negative and governed by SO_2 and Fe^{2+}, without evidence of additional synergistic amplification.

Based on the calibration conversion used in this study, the Mix1 bias corresponds to an atmospheric-scale uncertainty of approximately −0.056 ppbv for ROS_g and −0.006 μg m^{-3} for ROS_p, which is below the instrumental detection limits. The Mix2 bias corresponds to approximately −0.19 ppbv for ROS_g and −0.022 μg m^{-3} for ROS_p and represents a conservative high-level sensitivity scenario. Therefore, the quantified interference was unlikely to affect the seasonal pattern or pollution-regime interpretation of

the present field observations, although high-SO_2 or Fe-rich environments may lead to underestimation of ROS and should be further evaluated in future applications.

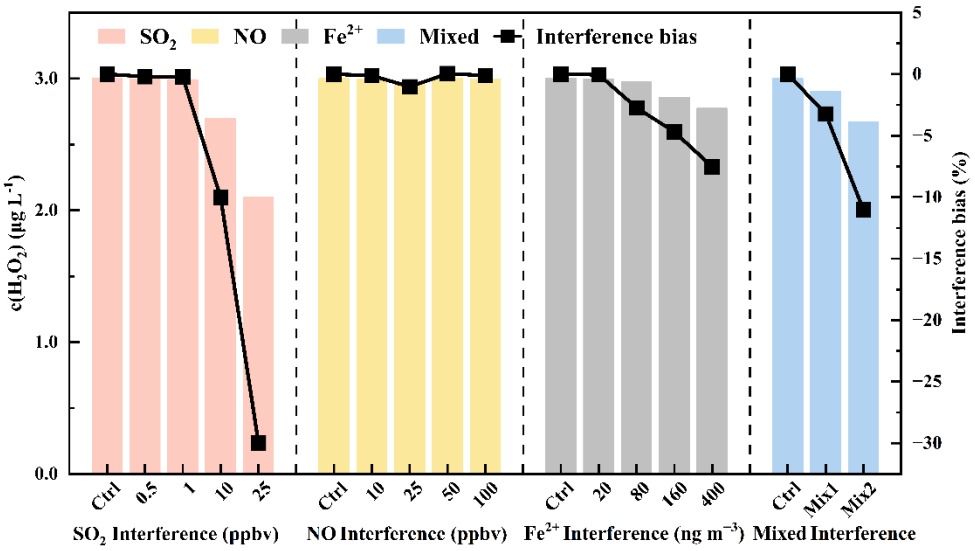

Figure 4. *Effects of SO_2, NO, Fe^{2+}, and mixed interferents on the DCFH-HRP response to 3 μg L^{-1} H_2O_2. SO_2 and NO levels are given in ppbv, and Fe^{2+} levels in ng m^{-3}. Mix1 contains 1 ppbv SO_2, 25 ppbv NO, and 80 ng m^{-3} Fe^{2+}, while Mix2 contains 10 ppbv SO_2, 100 ppbv NO, and 160 ng m^{-3} Fe^{2+}. Bars indicate measured H_2O_2-equivalent concentrations, and black squares indicate interference bias relative to the control.*

Comment 4: Correlation versus causation in the field interpretation. Several mechanistic interpretations in Section 4 rest on relatively weak correlations. Please provide p-values (or confidence intervals) and sample sizes, and consider tempering the mechanistic claims for relationships with |r| < 0.3.

Response 4: We appreciate this insightful comment on the limitations of correlation-based interpretation. We agree that correlation analysis alone cannot establish process-level causality, particularly for weak associations. Accordingly, **Figure 9** and the corresponding discussion in Sec. **4.3. Diurnal patterns of ROS under clean and polluted conditions** were revised to provide statistical support and to temper mechanistic interpretations based on weak correlations.

In the revised **Figure 9**, valid paired sample sizes are now reported for each seasonal and pollution-regime subset, and statistical significance is indicated using p-value thresholds: *p < 0.05, **p < 0.01,

and ***$p < 0.001$; correlations without asterisks indicate $p \geq 0.05$. The figure caption was also revised to specify that correlations with $|r| < 0.3$ are classified as weak associations.

The opening paragraph of Sec. **4.3. Diurnal patterns of ROS under clean and polluted conditions** was revised to clarify that the correlation analysis was used to evaluate covariation between ROS and individual atmospheric variables, whereas process-level interpretation was constrained by diurnal evolution, pollution-regime contrasts, and established atmospheric chemistry. All interpretations involving weak correlations were revised accordingly. In clean autumn, the weak ROS_g-O_3 association ($r = -0.15$) is now interpreted as indicating that O_3 alone did not explain ROS_g variability. In polluted autumn, the weak ROS_p-$PM_{2.5}$ association ($r = 0.28$) is now described as evidence that bulk particle mass alone could not account for ROS_p variability. For autumn evening conditions, the delayed ROS_g maximum relative to O_3 and its weak association with $PM_{2.5}$ are now used to indicate that ROS_g variability was not controlled by photochemistry alone. In winter, the weak ROS_p-$PM_{2.5}$ association ($r = 0.22$) and evening ROS_p rebound are framed as being consistent with heterogeneous and multiphase processing. For nocturnal summer conditions, ROS_p persistence despite weak $PM_{2.5}$ dependence ($r = 0.12$) is interpreted as evidence that bulk particle loading was not the primary driver. For clean winter, the weak associations of ROS_g with NO and NO_2 ($r = 0.06$-0.11) and of ROS_p with $PM_{2.5}$ ($r = 0.22$) are discussed together with nocturnal ROS_p persistence as being consistent with heterogeneous and aqueous-phase oxidation.

Revision in the manuscript:

The following text was revised in Sect. 4.3 Diurnal patterns of ROS under clean and polluted conditions:

Statement of the correlation analysis (line 457-458):

Figure 9 summarizes the covariation between ROS and key atmospheric species, with correlations of $|r| < 0.3$ classified as weak associations.

Clean autumn ROS_g-O_3 relationship (line 462-464):

ROS_g showed only a weak negative association with O_3 in clean autumn air ($r = -0.15$) (Figure 9),

indicating that O_3 alone did not explain ROS_g variability. The deviation between ROS_g and O_3 is consistent with additional influences from titration and precursor limitation in relatively clean air masses.

Polluted autumn ROS_p-$PM_{2.5}$ relationship (line 469-471):

In polluted autumn (Figure 8a), ROS_p was only weakly associated with $PM_{2.5}$ ($r = 0.28$), indicating that bulk particle mass alone could not account for ROS_p variability. This pattern points to a stronger influence of aerosol composition and secondary processing than by total particle mass, consistent with previous studies (Liu et al., 2023; Zhou et al., 2019; Huang et al., 2016).

Autumn evening ROS_g variation (line 480-484):

In autumn, the delayed ROS_g maxima relative to O_3, together with a weak positive association with $PM_{2.5}$ under polluted conditions ($r = 0.28$) (Figure 9), indicate that ROS_g variability was not controlled by photochemistry alone. Gas-particle coupling, boundary-layer evolution, and O_3-alkene reactions may have jointly contributed to sustaining oxidative capacity after peak photochemistry (Wang et al., 2023b).

Winter evening ROS_p variation (line 484-486):

In winter, declining ROS_g and weakly rebounding ROS_p in the evening, together with a weak positive association between ROS_p and $PM_{2.5}$ ($r = 0.22$) (Figure 9), are consistent with an increasing contribution from heterogeneous and multiphase processes as photochemical activity wanes (Xue et al., 2021).

Nocturnal summer ROS_p behavior (line 492-496):

Under clean winter and spring conditions (Figure 7b and 7c), ROS_g showed weak nocturnal variability, while ROS_p generally decreased in colder seasons but persisted or increased in summer despite weak $PM_{2.5}$ dependence ($r = 0.12$) (Figure 9), suggesting that bulk particle loading was not the primary driver of ROS_p variability. This behavior is compatible with continued multiphase ROS formation and aerosol aging under weak nocturnal photochemical forcing (Brown and Stutz, 2012; Wang et al., 2023a).

Clean winter ROS-precursor relationships (line 499-502):

Under clean winter conditions, ROS_g showed limited variability and only weak associations with NO and NO_2 (r = 0.06-0.11), while ROS_p also exhibited a weak positive association with $PM_{2.5}$ (r = 0.22) (Figure 9). Together with the nocturnal persistence of ROS_p, this pattern is consistent with a contribution from heterogeneous and aqueous-phase oxidation (Liu et al., 2023; Campbell et al., 2021).

The following text was revised in the Figure 9 caption (line 509-512):

Figure 9. *Seasonal correlations of ROS_g and ROS_p with key atmospheric species under clean and polluted conditions in each season. The numbers above each seasonal panel denote the number of valid paired observations after removal of missing values. Asterisks denote statistical significance: *$p < 0.05$, **$p < 0.01$, and ***$p < 0.001$; no asterisk indicates $p \geq 0.05$. Correlations with $|r| < 0.3$ are classified as weak associations.*

Comment 5: Mismatch between calibration range and ambient concentrations. The calibration covers atmospheric equivalents of 2.88–14.41 ppbv (ROS_g) and 0.29–1.49 μg m^{-3} (ROS_p), yet essentially all seasonal-mean field values fall below or close to the lowest calibration point. Low-concentration linearity is unverified; reagent auto-oxidation and blank-subtraction errors contribute proportionally more at low signal, and the near-zero-intercept calibration becomes sensitive to small intercept errors. I recognize the campaign has concluded; nonetheless, it would be valuable to perform a low-range verification at the current instrument state and use any campaign QA/QC records to constrain drift.

Response 5: We indeed appreciate the reviewer's insight into the study. We agree that the seasonal-mean ROS_g and ROS_p concentrations were close to the lower end of the original calibration range, and that blank subtraction, reagent auto-oxidation, and small intercept uncertainty become proportionally more important at low signal levels.

To directly address this concern, we performed an additional low-concentration verification experiment using the current instrument configuration. Two low-concentration H_2O_2 standards, 1.0 and 3.0 μg L^{-1}, were added to the original calibration sequence. These standards correspond to atmospheric-equivalent concentrations of approximately 0.58 and 1.73 ppbv for ROS_g, and 0.066 and 0.20 μg m^{-3} for ROS_p, respectively. The new experimental results were incorporated into the revised manuscript and Fig. 3d to

verify the instrument response below the original calibration boundary.

Accordingly, in Sect. **2.4 Instrument calibration**, we clarified the blank-corrected quantification procedure. Specifically, we stated that a blank-corrected through-origin working curve was used, and that the blank signal was subtracted from the measured fluorescence signal before concentration calculation. This revision clarifies that zero ROS concentration corresponds to zero net fluorescence response.

In addition, in Sect. **3.2.3 Sensitivity and response time**, we added the newly performed low-concentration switching experiment. The added 1.0 and 3.0 μg L^{-1} H_2O_2 standards produced distinguishable and stable signal responses above the blank baseline, confirming that the instrument could resolve concentration changes near the lower ambient range.

Based on these new experimental results, in Sect. **3.2.4 Linear working range**, we revised the calibration description based on the newly added experimental results. The verified calibration range was expanded from 5.0-25.0 μg L^{-1} to 1.0-25.0 μg L^{-1} H_2O_2. The updated baseline-corrected calibration showed linear responses in both channels, with through-origin working curves of y = 0.111x for ROS_g and y = 0.125x for ROS_p. This additional low-range experiment directly verifies the low-concentration linearity that was not demonstrated in the original manuscript.

Consistently, in **Fig. 3d**, we added the new low-concentration calibration points and the corresponding time-resolved switching signals. The inset now shows the response sequence including 1.0 and 3.0 μg L^{-1} H_2O_2, demonstrating that the low-level signals were clearly resolved from the blank baseline.

Finally, in Sect. **4.2 Overall variations of ROS and associated atmospheric species**, we added a direct comparison between the lowest seasonal mean concentrations and the newly verified calibration range. The lowest seasonal mean concentrations reported in this study, 1.03 ppbv for ROSg and 0.17 μg m^{-3} for ROSp, fall within the expanded calibration range. These values also exceeded the corresponding 3σ detection limits by factors of approximately 15 and 25, respectively. In addition, the 10 h blank test showed a baseline RSD of 0.37%, and the repeated 20 μg L^{-1} H_2O_2 standard test showed an RSD of 0.57%. Together, the newly added low-concentration experiment, stable blank behavior, and repeated-standard results confirm that the low-level ambient signals were analytically resolved rather than artifacts of blank noise or short-term instrumental drift.

Revision in the manuscript:

The following text was revised in Sect. 2.4 Instrument calibration (line 189-191):

A blank-corrected through-origin working curve was used for quantification; the blank signal was subtracted from the measured fluorescence signal prior to concentration calculation, thereby defining zero ROS concentration as zero net fluorescence response.

The following text was revised in Sect. 3.2.3 Sensitivity and response time (line 295-296):

Standards of 1.0, 3.0, 5.0, 10.0, 20.0, and 25.0 μg L^{-1} correspond to ROS_g of 0.58, 1.73, 2.88, 5.76, 11.52, and 14.41 ppbv, and ROS_p of 0.07, 0.20, 0.33, 0.66, 1.33, and 1.66 μg m^{-3}.

The following text and figure were revised in Sect. 3.2.4 Linear working range (line 300-311):

The linear working range was determined by simultaneous injection and switching tests in the gas and particle phase channels using the same H_2O_2 standards (1.0-25.0 μg L^{-1}). Regression analysis showed a strong linear relationship between the baseline-corrected fluorescence response and standard concentration. A through-origin working curve was used for quantification, with $y \approx 0.1x$ and $R^2=0.99$ (Figure 3d). The two channels exhibited nearly identical response behavior, calibration slopes, and response times, indicating strong inter-channel agreement and stable system matching. The RSD at each concentration point was below 1%, supporting robust quantitative performance within the tested range. The atmospheric-equivalent calibration range was 0.58-14.41 ppbv for ROS_g and 0.07-1.66 μg m^{-3} for ROS_p. Together with the stable blank behavior and low detection limits, this calibration provides the quantitative basis for subsequent ambient measurements, while measurements near the lower calibration boundary are interpreted with appropriate consideration of blank-related uncertainty.

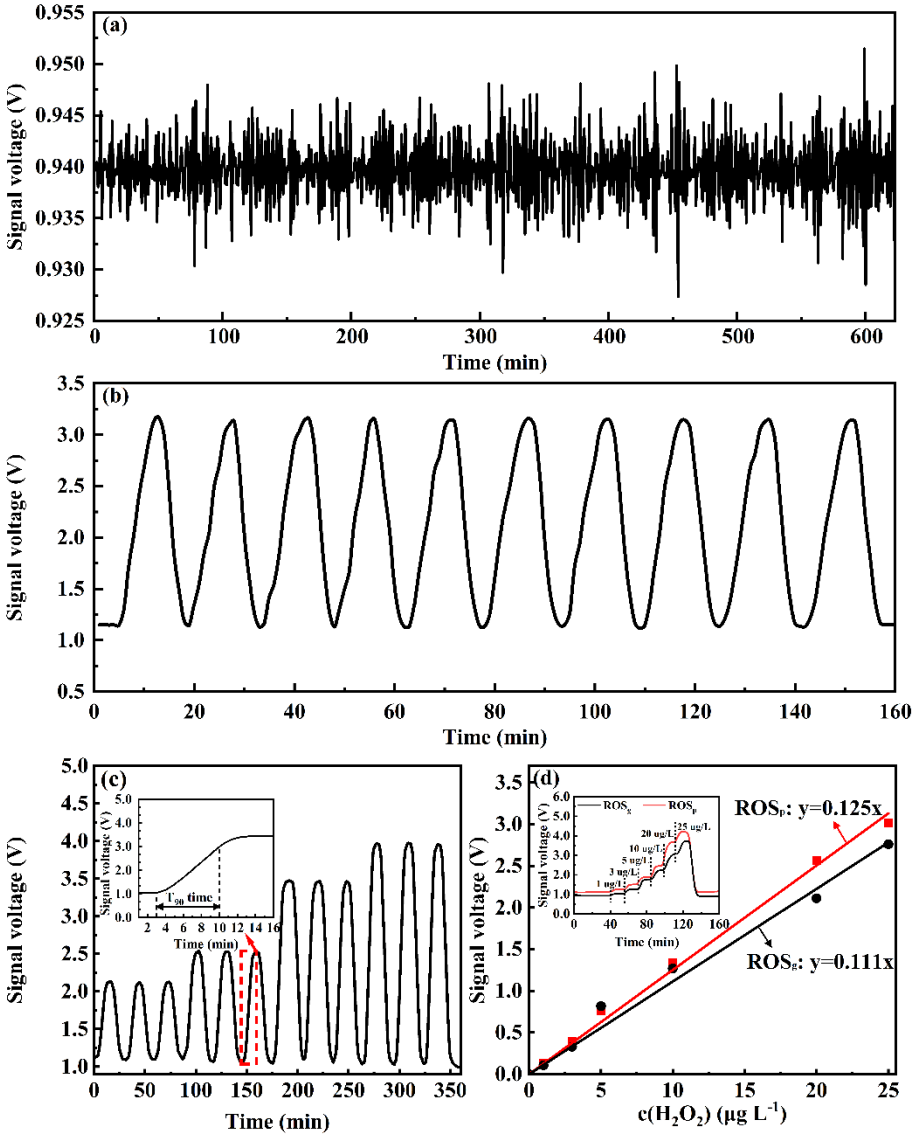

Figure 3. *Performance evaluation of the atmospheric ROS online analyzer: (a) baseline stability, (b) reproducibility, (c) sensitivity, and (d) linear working range.*

The following text was revised in Sect. 4.2 Overall variations of ROS and associated atmospheric species (line 401-405):

The lowest seasonal mean concentrations were within the verified linear response range of the instrument, which covered the corresponding atmospheric-equivalent levels of the field observations. These values also exceeded the corresponding 3σ detection limits by factors of approximately 15 and 24 for ROS_g and ROS_p, respectively, confirming that the seasonal-average signals were analytically resolved rather than artifacts of instrumental blank noise or short-term instrumental drift.

Comment 6: Contradiction with previous Beijing observations. Huang et al. (2016), using a closely related instrument at a rural Beijing site, found ROS higher in winter than spring; the present study (urban Beijing) finds spring highest and autumn lowest. Please discuss the possible reasons for the opposite seasonal ranking.

Response 6: In response to this comment, we have revised the spring discussion in Sect. **4.2 Overall variations of ROS and associated atmospheric species** to explicitly address this difference. Huang et al. (2016) reported higher winter than spring ROS at a rural Beijing site, where winter ROS was likely enhanced by heating-related emissions, higher $PM_{2.5}$ loading, and stagnant meteorological conditions, while the spring campaign was characterized by relatively good air quality without haze episodes. In contrast, our spring observations at an urban Beijing site showed enhanced ROS_g from 2.10 ppbv on clean days to 3.02 ppbv on polluted days, accompanied by elevated O_3 and $j(O^1D)$, indicating a stronger O_3-driven photochemical regime. Therefore, the spring maximum in the present study does not contradict Huang et al. (2016), but reflects differences in site type and seasonal pollution regime: winter particle accumulation and combustion-related effects were more important in their rural observations, whereas springtime photochemical ROS production was more pronounced in our urban observations.

Revision in the manuscript:

The following text was added to Sect. 4.2 Overall variations of ROS and associated atmospheric species (line 430-438):

In spring, ROS_g increased from 2.10 ppbv on CDs to 3.02 ppbv on PDs, accompanied by higher O_3 (39.35-60.21 ppbv) and $j(O^1D)$ (4.52×10^{-6}-7.13×10^{-6} s^{-1}), indicating an O_3-driven photochemical regime. This seasonal maximum contrasts with previous rural Beijing observations, where spring ROS was lower than winter ROS under relatively clean, haze-free spring conditions, which limited haze-related precursor accumulation and radical formation (Huang et al., 2016). In the present urban observations, stronger spring photolysis and elevated O_3 instead favored gas-phase ROS production, explaining why spring ROS exceeded winter levels. ROS_p remained comparably high on CDs and PDs (0.50 μg m^{-3}), suggesting that, once photochemistry was sufficiently active, particle oxidative activity could be sustained despite lower aerosol loading through continued production and uptake of peroxides and other semi-volatile oxidants and in-particle transformation pathways (Huang et al., 2016; Zhou et al., 2019).

Minor Comments:

Comment 1: Eq. 2.3. The factor $(T_0/T)(P_0/P)$ appears inverted; it should read $(T_0/T)(P/P_0)$. Please correct and confirm whether the reported ROS_g values were affected.

Response 1: We thank the reviewer for carefully checking the unit conversion equation and for pointing out this mistake. We have corrected Eq. (2.3) in Sect. **2.4 Instrument calibration** by replacing the pressure correction term in the denominator from (P_0/P) to (P/P_0). We also rechecked the original data-processing files and confirmed that the ROS_g concentrations reported in the manuscript were calculated using the correct conversion factor. Therefore, this error only affected the written form of Eq. (2.3), and the reported ROS_g values, figures, tables, and conclusions were not affected.

Revision in the manuscript:

The following text was revised in Sect. 2.4 Instrument calibration (line 198):

$$C_{ROS_g}\,(ppbv) = \frac{C_{ROS}\,(\mu g\ m^{-3})V_m}{M(T_0/T)(P/P_0)} \qquad (2.3)$$

Comment 2: Table 1. The bolded optimal row for temperature effects is 37 °C, whereas the text (line 234) states 40 °C was selected. Please reconcile.

Response 2: Thank you for pointing out this inconsistency. The discrepancy was caused by a formatting error in Table 1, where the 37 ºC row was inadvertently bolded. The intended and experimentally selected optimal temperature was 40 ºC, as stated in the text. Compared with 37 °C, 40 °C showed a slightly higher calibration-curve slope (0.079 vs. 0.078) and a lower baseline SD (0.004 vs. 0.005), indicating better measurement stability while maintaining high sensitivity. Therefore, 40 ºC was selected as the optimal reaction temperature. We have corrected Table 1 in Sect. **3 Instrument assessment** by moving the bold formatting from the 37 ºC row to the 40 ºC row. This was only a table-formatting error and did not affect the experimental procedure, data analysis, or reported results.

Revision in the manuscript:

The following table was revised in Sect. 3 Instrument assessment (line 267):

Table 1. *Optimization of DCFH-HRP fluorescence detection conditions*

Category	*Parameter*		*Standard curve*	*Baseline SD*
	c(HRP) (units mL^{-1})	*c(DCFH) (μmol L^{-1})*		
A. Reagent concentrations	*0.5*	*10*	*y=0.068x; R^2=0.996*	*0.003*
	0.5	*20*	*y=0.080x; R^2=0.992*	*0.006*
	0.5	*40*	*y=0.093x; R^2=0.996*	*0.008*
	1.0	*10*	*y=0.063x; R^2=0.995*	*0.003*
	1.0	*20*	*y=0.072x; R^2=0.985*	*0.005*
	1.0	*40*	*y=0.080x; R^2=0.999*	*0.007*
	2.0	***10***	***y=0.089x; R^2=0.996***	***0.002***
	2.0	*20*	*y=0.090x; R^2=0.992*	*0.009*
	2.0	*40*	*y=0.096x; R^2=0.999*	*0.006*
B . Temperature effects	*Temperature (°C)*			
	30		*y=0.076x; R^2=0.994*	*0.009*
	33		*y=0.078x; R^2=0.996*	*0.011*
	37		*y=0.078x; R^2=0.998*	*0.005*
	40		***y=0.079x; R^2=0.999***	***0.004***
C. Photoelectric detection effects	*PMT voltage (V)*	*LED current (mA)*		
	600	*8*	*y=0.108x; R^2=0.996*	*0.011*
	700	***6***	***y=0.107x; R^2=0.998***	***0.005***
	800	*4*	*y=0.105x; R^2=0.992*	*0.006*
	900	*2*	*y=0.104x; R^2=0.995*	*0.006*

Comment 3: A short paragraph acknowledging the methodological limitations would be a useful addition in the conclusion section.

Response 3: We are very thankful for the reviewer's helpful suggestion. We have added a concise paragraph at the end of the Sect. **5 Conclusions** to acknowledge the methodological limitations of the present analyzer. The added text clarifies that the DCFH-HRP assay provides operational H_2O_2-equivalent ROS concentrations with species-dependent responses, rather than molecule-specific or total atmospheric ROS. We also noted that, although the observation-constrained interference budget suggested minor effects under the present campaign conditions, the response-function-based interference assessment should be further validated using mixed-interferent tests under broader atmospheric matrices. In addition, we clarified that the ROS_p collection efficiency was determined from triplicate recovery experiments under ambient aerosol sampling conditions, and that its potential dependence on particle loading, hygroscopic growth, aerosol composition, and extended field operation remains an important aspect for future evaluation.

Revision in the manuscript:

The following text was added to Sect. 5 Conclusions (line 588-597):

These findings demonstrate the capability of the analyzer to resolve phase-dependent ROS variability under contrasting urban pollution regimes, while their interpretation should remain within the operational scope of the method. Specifically, the DCFH-HRP assay reports H_2O_2-equivalent ROS with species-dependent responses, rather than molecule-specific or total atmospheric ROS. Direct interference tests showed that NO caused negligible bias, whereas elevated SO_2 and Fe^{2+} could introduce negative interferences. The environmentally representative mixed-interferent condition produced only a small bias close to or below the instrumental detection limits, indicating that the quantified interference was unlikely to affect the field interpretation. Nevertheless, high-SO_2 or Fe-rich environments may lead to ROS underestimation and should be further evaluated. In addition, the ROS_p collection efficiency was determined from triplicate recovery experiments under actual ambient aerosol sampling conditions; its potential dependence on particle loading, hygroscopic growth, aerosol chemical composition, and extended field operation should be further evaluated in future applications.

Reference:

Hua, W., Chen, Z., Jie, C., Kondo, Y., Hofzumahaus, A., Takegawa, N., Chang, C., Lu, K., Miyazaki, Y., and Kita, K.: Atmospheric hydrogen peroxide and organic hydroperoxides during PRIDE-PRD'06, China: their concentration, formation mechanism and contribution to secondary aerosols, Atmospheric Chemistry and Physics, 8, 6755-6773, https://doi.org/10.5194/acp-8-6755-2008, 2008.

Huang, W., Zhang, Y., Zhang, Y., Zeng, L., Dong, H., Huo, P., Fang, D., and Schauer, J. J.: Development of an automated sampling-analysis system for simultaneous measurement of reactive oxygen species (ROS) in gas and particle phases: GAC-ROS, Atmospheric environment, 134, 18-26, https://doi.org/10.1016/j.atmosenv.2016.03.038, 2016.

King, L. E. and Weber, R. J.: Development and testing of an online method to measure ambient fine particulate reactive oxygen species (ROS) based on the 2', 7'-dichlorofluorescin (DCFH) assay, Atmospheric Measurement Techniques, 6, 1647-1658, https://doi.org/10.5194/amt-6-1647-2013, 2013.

Kolthoff, I. M. and Medalia, A. I.: The reaction between ferrous iron and peroxides. I. Reaction with hydrogen peroxide in the absence of oxygen, Journal of the American Chemical Society, 71, 3777-3783, https://doi.org/10.1021/ja01179a057, 1949.

Komazaki, Y., Inoue, T., and Tanaka, S.: Automated measurement system for H_2O_2 in the atmosphere by diffusion scrubber sampling and HPLC analysis of Ti (IV)-PAR-H_2O_2 complex, Analyst, 126, 587-593, https://doi.org/10.1039/B008134P, 2001.

Lazrus, A. L., Kok, G. L., Lind, J. A., Gitlin, S. N., Heikes, B. G., and Shetter, R. E.: Automated fluorometric method for hydrogen peroxide in air, Analytical chemistry, 58, 594-597, https://doi.org/10.1021/ac00294a024, 1986.

Montesinos, V. N., Sleiman, M., Cohn, S., Litter, M. I., and Destaillats, H.: Detection and quantification of reactive oxygen species (ROS) in indoor air, Talanta, 138, 20-27, https://doi.org/10.1016/j.talanta.2015.02.015, 2015.

Zhou, J., Bruns, E. A., Zotter, P., Stefenelli, G., Prévôt, A. S., Baltensperger, U., El-Haddad, I., and Dommen, J.: Development, characterization and first deployment of an improved online reactive oxygen species analyzer, Atmospheric Measurement Techniques, 11, 65-80, https://doi.org/10.5194/amt-11-65-2018, 2018.